Journal of Membrane Science 642 (2022) 119978

Contents lists available at ScienceDirect

Journal of Membrane Science

journal homepage: www.elsevier.com/locate/memsci

High-temperature hydrogen/propane separations in asymmetric carbon molecular sieve hollow fiber membranes

Lu Liu, Dongxia Liu **, Chen Zhang *

Department of Chemical and Biomolecular Engineering, University of Maryland, 4418 Stadium Drive, College Park, MD, 20742, United States

ARTICLE INFO

Keywords:
Carbon molecular sieve membrane
High-temperature separation
Membrane reactor
Hollow fiber membrane
Hydrogen/propane separation

ABSTRACT

Catalytic propane dehydrogenation membrane reactors require membranes with highly attractive high-temperature H_2/C_3H_8 separation performance. In this work, we show that polyimide-derived asymmetric carbon molecular sieve (CMS) hollow fiber membranes with thin (~5 μm) separation layers can provide outstanding high-temperature (up to 600 °C) H_2/C_3H_8 separation factors 2–100 folds higher than microporous oxide membranes. The effects of CMS membrane pyrolysis condition, permeation temperature, and feed composition on high-temperature H_2/C_3H_8 separation performance were systematically investigated. CMS hollow fiber membranes pyrolyzed at 675 °C showed stable H_2 permeance of 430 GPU and H_2/C_3H_8 separation factor of 511 at 600 °C using a 50%/50% H_2/C_3H_8 feed mixture under a continuous permeation test of ~130 h. It was found that CMS membrane pore structure and separation performance may be modulated by hydrogenation and coke deposition by the H_2/C_3H_8 mixture under high-temperature permeation. A trade-off between these two potential reactions is achieved by controlling H_2/C_3H_8 compositions, leading to stable CMS under high-temperature conditions. The results suggest that asymmetric CMS hollow fiber membranes are potentially attractive for catalytic propane dehydrogenation membrane reactors under controlled high-temperature reaction conditions.

1. Introduction

Large-scale membrane gas and vapor separations are rarely practiced at temperatures above 200 °C. This is mostly due to a lack of scalable high-temperature separation membranes rather than the need for high-temperature membrane applications. Catalytic membrane reactors are among the potential applications of high-temperature membrane separation. By removing one or more reaction products, catalytic membrane reactors integrate chemical conversion and separation providing enhanced conversion of reversible reactions based on the Le Chatelier's principle [1]. High-temperature catalytic membrane reactors have been studied for hydrocarbon dehydrogenation [2,3], water-gas shift reaction [4,5], methanol steam reforming [6], CO_2 hydrogenation [7,8], and methane conversion [9–11]. Notably, propane dehydrogenation (PDH) membrane reactors are of particular interest for on-purpose propylene production [12]. Propane dehydrogenation is an equilibrium limited reaction with heat of reaction (298 K) of 124.3 kJ/mol. Commercial PDH reactors are carried out above 525 °C to enhance C_3H_8 conversion, which often causes catalyst deactivation by coking [13]. By selectively removing H_2, PDH membrane reactors can potentially achieve economically attractive C_3H_8 conversion at lower reaction temperatures with mitigated catalyst coking. Hydrogen-permeable membranes with attractive high-temperature H_2/C_3H_8 separation performance are crucial to provide enhanced C_3H_8 conversion and minimized C_3H_8 loss in PDH membrane reactors. Inorganic membranes (e.g., zeolite, microporous silica, metallic, and ion-transport ceramic) have outstanding high-temperature stability and can enhance propane conversion in PDH membrane reactors [14–21]. This fact notwithstanding, no PDH membrane reactors are used at large-scale due to inadequate scalability of most inorganic membranes.

Carbon molecular sieve (CMS) membranes have been studied for gas and vapor separations due to their unique balance of high separation performances and good scalability [22,23]. Pilot-scale demonstrations of CMS hollow fiber membranes have been reported for off-shore natural gas purification [24]. Recently, Lei and co-workers showed the feasibility to produce high-purity H_2 in a two-stage CMS hollow fiber

* Corresponding author. Department of Chemical and Biomolecular Engineering, University of Maryland, 4418 Stadium Drive, College Park, MD, 20742, United States.;

** Corresponding author. Department of Chemical and Biomolecular Engineering, University of Maryland, 4418 Stadium Drive, College Park, MD, 20742, United States.

E-mail addresses: liud@umd.edu (D. Liu), czhang71@umd.edu (C. Zhang).

https://doi.org/10.1016/j.memsci.2021.119978
Received 3 May 2021; Received in revised form 27 September 2021; Accepted 12 October 2021
Available online 14 October 2021
0376-7388/© 2021 Elsevier B.V. All rights reserved.

membrane system [25]. CMS membranes are derived by carbonization of polymer precursors above their decomposition temperatures under inert atmosphere or vacuum, which results in graphene layers packed imperfectly to form a disordered pore structure [26]. Molecular transport in CMS membrane is controlled by its disordered pore structure often described by the bimodal pore size distribution, where the slit-like pores are comprised of micropore "chambers" (7–20 Å) and ultramicropore "windows" (<7 Å) [26]. This unique pore structure gives CMS membranes simultaneous high productivity and high separation efficiency exceeding those of polymer membranes [27] and competitive with many inorganic membranes [28]. The pore structure and separation performance of CMS membranes can be controlled by rational design of polymer precursor chemistry [29–32]. Owing to their excellent tunability, CMS membranes have shown attractive separation performance for many economically important gas [33], vapor [34,35], and organic solvent separations [36] at ambient temperatures.

Due to excellent thermal resistance and chemical stability, CMS membranes are promising candidates for high-temperature gas and vapor separations. Sznejer and co-workers reported attractive hydrogen/hydrocarbon separation factors in dense-wall symmetric CMS hollow fiber membranes at temperatures up to 400 °C [37]. Itoh and Haraya studied a hydrogen-permeable CMS membrane reactor for non-oxidative cyclohexane dehydrogenation at 195 °C using a polyimide-derived CMS membrane [38]. The results showed cyclohexane conversion in the CMS membrane reactor exceeded the thermodynamic equilibrium conversion. Hydrogen-permeable CMS membrane reactors were also investigated for non-oxidative *iso*-butane dehydrogenation [39], non-oxidative methyl-cyclohexane dehydrogenation [40], water gas shift reaction [41,42], and methanol steam reforming [43,44]. It should be noted that the permeation temperature in these CMS membrane reactor studies usually do not exceed ~500 °C. CMS membranes have not been studied for propane dehydrogenation membrane reactors, which require higher permeation temperatures above 500 °C. In addition, systematic studies of CMS membrane high-temperature permeation properties are lacking. Several of the aforementioned CMS membrane reactor studies use CMS membranes supported on thick (diameter 6–10 mm) ceramic tubular supports. With much smaller diameters (~0.1–1 mm) and thin separation layers (0.5–5 μm), the recently emerged asymmetric CMS hollow fiber membranes [45] and composite CMS hollow fiber membranes [46,47] can provide much higher membrane packing density and permeances [48,49]. They are more attractive than tubular CMS/ceramic structures for high-temperature catalytic membrane reactor applications.

In this work, we aim to explore the high-temperature gas separation performance of asymmetric CMS hollow fiber membranes in non-oxidative propane dehydrogenation conditions. We systematically studied H_2/C_3H_8 separation in hydrogen-permeable polyimide-derived asymmetric CMS hollow fiber membranes with thin separation layers (~5 μm) at permeation temperature up to 600 °C. The roles of membrane pyrolysis condition and permeation temperature on high-temperature H_2/C_3H_8 separation performance were investigated. The Arrhenius equation was used to calculate CMS membrane intrinsic permeation properties using measured average permeances. We also studied the effects of feed composition on high-temperature H_2/C_3H_8 separation performance of CMS hollow fiber membranes. The results allowed us to understand the effects of high-temperature H_2 and C_3H_8 exposure on CMS pore structure and transport properties. Finally, a continuous ~130-h permeation test was carried out at 600 °C to demonstrate the outstanding long-term stability of CMS hollow fiber membrane performance under high-temperature permeation. The present study forms a basis for the development of CMS membrane reactors for propane dehydrogenation chemistry. The materials and concepts are applicable to other direct non-oxidative hydrocarbon activations such as ethane and methane upgrading reactions.

2. Theory and background

Transport in CMS membranes follows the sorption-diffusion mechanism [50]. Permeability is a measure of membrane intrinsic productivity and is defined as partial pressure difference and membrane thickness normalized flux. The separation layer thickness of asymmetric hollow fiber membranes usually cannot be unambiguously determined, and permeance (P_i/l) is often used to describe the membrane productivity, which is defined as partial pressure difference (Δp_i) normalized flux (J_i)

$$\left(\frac{P_i}{l}\right) = \frac{J_i}{\Delta p_i} \tag{1}$$

where P_i is the permeability of component i and l is membrane separation layer thickness. The units often used for permeability and permeance are Barrer and gas permeation unit (GPU), respectively

$$1 \text{ Barrer} = 10^{-10}\frac{\text{cm}^3(\text{STP})\cdot\text{cm}}{\text{cm}^2\cdot\text{s}\cdot\text{cmHg}} \tag{2}$$

$$1 \text{ GPU} = 10^{-6}\frac{\text{cm}^3(\text{STP})}{\text{cm}^2\cdot\text{s}\cdot\text{cmHg}} \tag{3}$$

Selectivity is a measure of membrane separation efficiency. The ideal permselectivity of a membrane with negligible downstream pressure is defined as the ratio of permeabilities or permeances

$$\alpha_{A/B} = \frac{P_A}{P_B} = \frac{P_A/l}{P_B/l} \tag{4}$$

With mixture feed, separation factor is often used to describe membrane separation efficiency

$$\alpha_{A/B} = \frac{y_A/y_B}{x_A/x_B} \tag{5}$$

where y and x are molar composition at membrane permeate side and retentate side, respectively. Permeability can further be written as the product of diffusivity D_i and sorption coefficient S_i

$$P_i = D_i \cdot S_i \tag{6}$$

The temperature dependence of diffusivities can be described by the Arrhenius relationship (Eqn. (7)). The temperature dependence of sorption coefficients can be described using the van't-Hoff equation (Eqn. (8)) [51].

$$D_i = D_{i0} \exp\left(-\frac{E_{D,i}}{RT}\right) \tag{7}$$

$$S_i = S_{i0} \exp\left(-\frac{\Delta H_{S,i}}{RT}\right) \tag{8}$$

where D_{i0} and S_{i0} are pre-exponential factors, R is the universal gas constant (J/mol/K), and T is the absolute temperature (K), $E_{D,i}$ is the activation energy for diffusion (kJ/mol) and $\Delta H_{S,i}$ is the heat of sorption (kJ/mol). According to Eqns. (6)–(8), the temperature dependence of permeance follows an Arrhenius relationship

$$\left(\frac{P_i}{l}\right) = \left(\frac{P_{i0}}{l}\right)\exp\left(-\frac{E_{P,i}}{RT}\right) \tag{9}$$

where P_{i0}/l is the pre-exponential factor and $E_{P,i}$ is the apparent activation energy for permeation (kJ/mol)

$$E_{P,i} = E_{D,i} + \Delta H_{S,i} \tag{10}$$

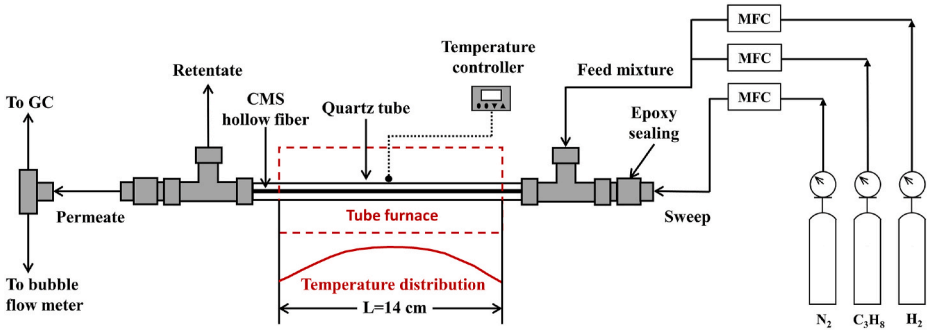

Fig. 1. Schematic illustration of the high-temperature H_2/C_3H_8 permeation system. (MFC: mass flow controller).

3. Experimental methods

3.1. Materials

Matrimid® 5218 polyimide was provided by Huntsman Corporation (Salt Lake City, UT). Vinyltrimethoxysilane (VTMS, 97%), *N*-Methyl-2-pyrrolidone (NMP, anhydrous, 99.5%), tetrahydrofuran (THF, anhydrous, 99.5%), ethanol (anhydrous, 99.5%), and hexane (mixture of isomers, anhydrous, 99%) were obtained from Sigma Aldrich (St. Louis, MO). Methanol (99.8% ACS, VWR Chemicals BDH®) and hexane (98.5% ACS, Millipore Sigma) were used for precursor hollow fiber solvent exchange. All chemicals were used as received.

3.2. Formation of precursor hollow fiber membranes

Monolithic Matrimid® precursor hollow fiber membranes were fabricated using dry-jet/wet-quench fiber spinning [52,53] with a custom-built hollow fiber spinning system. Matrimid® 5218 polyimide powder was dried under vacuum at 110 °C for 15 h for moisture removal. The polymer dope composition [54] and spinning parameters are shown in Table S1. The as-spun precursor hollow fiber membranes were soaked in three separate deionized water baths over the course of 72 h and solvent exchanged with three separate 20 min methanol baths followed by three separate 20 min hexane baths. After being dried in a fume hood overnight, the precursor hollow fibers were dried under vacuum at 75 °C for 12 h.

3.3. Formation of CMS hollow fiber membranes

The precursor hollow fibers were treated by VTMS to resist substrate collapse during pyrolysis. The precursor hollow fibers were soaked in a 10 wt% VTMS/hexane solution for 24 h and then exposed to water-vapor saturated air for another 24 h at room temperature. The VTMS-treated precursor hollow fibers were vacuum dried at 150 °C for 12 h prior to pyrolysis [45]. Pyrolysis of VTMS-treated precursor hollow fibers was performed in a three-zone tube furnace (MTI Corporation, Richmond, CA). The precursor hollow fibers were placed on a stainless-steel wire mesh (McMaster Carr, Robbinsville, NJ) in a quartz tube (MTI Corporation, Richmond, CA) and then loaded into the furnace. Ultra-high purity (UHP) argon was introduced to the quartz tube at 200 cc/min using a mass flow controller (MTI Corporation, Richmond, CA). The oxygen level in the system was kept below 5 ppm prior to pyrolysis, which was monitored by an oxygen analyzer (Cambridge Sensotec, Saint Ives, UK). The heating protocol below was used for pyrolysis:

1) Room temperature to 250 °C, 13.3 °C/min
2) 250 to T_{final}-15, 3.85 °C/min (T_{final} = 550, 675, or 800 °C)
3) T_{final}-15 to T_{final}, 0.25 °C/min
4) Dwelling at T_{final} for 2 h
5) Cooling down naturally to room temperature

3.4. Formation of CMS dense films

Matrimid® polymer precursor dense films were formed by solution casting [55]. Dried Matrimid® powders were dissolved in THF to prepare a ~20 wt% polymer solution. A nascent polymer film was obtained by knife-casting the polymer solution on a glass plate inside a THF saturated glove bag (Glas-Col, Terre Haute, IN). Following solvent evaporation, the film was removed from the glass plate and dried under vacuum at 110 °C for 12 h. CMS dense films were formed by pyrolysis of the Matrimid® polymer precursor dense films at 675 °C using the identical pyrolysis protocol with the aforementioned CMS hollow fiber membranes.

3.5. Construction of CMS hollow fiber membrane modules

CMS hollow fiber membrane modules were constructed following a similar procedure described in the literature [56]. Quartz tube (Quartz Scientific Inc. Fairport Harbor, OH) and stainless steel ultratorr fittings (Swagelok, Solon, OH) were used for the module construction. The length of the hollow fiber module was ~40 cm. Each module contained a single CMS hollow fiber. Epoxy (3M™ Scotch-Weld™ DP-100) was used as sealing. During high-temperature permeation, the Epoxy-sealed module connections were kept outside the furnace and exposed to ambient conditions.

3.6. High-temperature permeation measurements

The separation performance of CMS hollow fiber membranes was evaluated by a custom high-temperature permeation system (Fig. 1), in which the desired permeation temperature was achieved by heating the quartz tube portion of the hollow fiber module by a 14-cm single-zone tube furnace (DS Fibertech Corporation, Santee, CA). During the temperature ramping, inert gas (N_2) was introduced to hollow fiber shell and bore sides to prevent membrane decomposition by air. The stability of CMS membranes under high temperature inert gas was verified by mass spectrometry (Fig. S1). Once the temperature reached the target value, a H_2/C_3H_8 feed mixture (1 bar, 30 cc/min) was introduced to the hollow fiber shell side while N_2 sweep gas (10 cc/min) was introduced to the hollow fiber bore side. Permeate flow rate was measured using a bubble flow meter and permeate compositions were analyzed by an Agilent-6890 gas chromatograph (GC). A thermal conductivity detector (TCD) and a packed column (HayeSep DB, Agilent) were used for H_2 detection. A flame ionization detector (FID) and a capillary column (GS-GasPro, Agilent) were used for C_3H_8 detection. Permeation data were continuously collected until the GC readings became stabilized for at least 3 h. Each permeation measurement was run for a minimum of 24 h.

Since heating provided by the single-zone furnace was not uniform (Fig. 1), average permeances and average separation factors were obtained by the permeation measurements. As the module temperature dramatically drops outside the furnace and membrane permeance drops exponentially with temperature (Eqn. (9)), only permeation from the

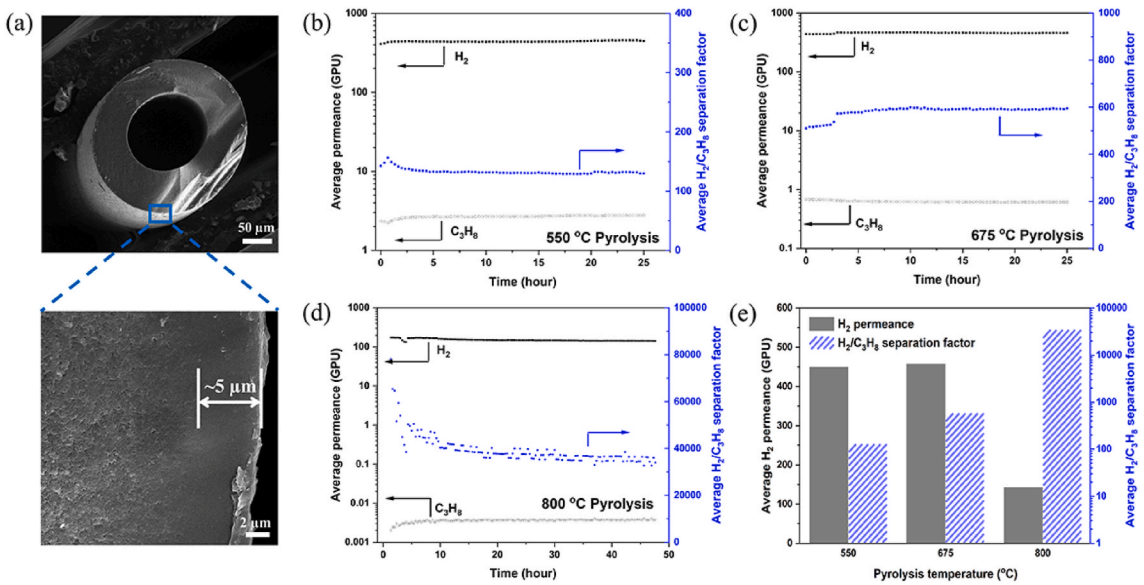

Fig. 2. (a) SEM images of an asymmetric CMS hollow fiber membrane; H_2/C_3H_8 permeation results in CMS hollow fiber membranes pyrolyzed at (b) 550 °C, (c) 675 °C, and (d) 800 °C; (e) Stabilized average permeances and separation factors. The permeation measurements were performed at 600 °C (furnace set temperature) using a 50%H_2/50%C_3H_8 feed mixture (1 bar).

hollow fiber module inside the furnace was considered for permeance calculations. The measured average permeances were used to calculate apparent permeation activation energies

$$P_{i,\ average} = \frac{1}{L}\int_{-\frac{L}{2}}^{\frac{L}{2}} P_{i0}\exp\left(\frac{E_{P,i}}{RT(z)}\right)dz \tag{11}$$

where $P_{i,\ average}$ is the measured average permeance of component i, $T(z)$ is the measured temperature distribution profile, L is furnace length ($L = 14$ cm) and z is the location ($z = 0$ cm at the center of the furnace). With the average permeances and temperature distribution profiles measured at different furnace set temperatures, the apparent permeation activation energies can be calculated by the least-squares method.

3.7. Characterizations

The morphology of CMS hollow fiber membranes was examined by a XEIA3 TESCAN scanning electron microscope (SEM) with an operating voltage of 10 kV. CO_2 physisorption isotherms (273.15 K) were measured using an ASAP 2020PLUS physisorption analyzer (Micromeritics, Norcross, GA). The density functional theory (slit pores) was used to calculate the pore size distribution, pore surface area, and pore volume using the measured CO_2 physisorption isotherms.

4. Results and discussion

4.1. Effects of pyrolysis temperature on high-temperature H_2/C_3H_8 separation performance

Catalytic membrane reactors require membranes with a balance of attractive permeance and separation factor. While high permeances are useful to provide enhanced conversion, outstanding separation factors are needed to minimize reactant loss. We studied the effects of pyrolysis temperature on controlling high-temperature H_2/C_3H_8 separation performance of CMS hollow fiber membranes. Monolithic Matrimid® precursor hollow fibers were fabricated using dry-jet/wet-quench hollow fiber spinning (Fig. S2). Asymmetric CMS hollow fiber membranes were derived from the precursor hollow fibers by pyrolysis at 550, 675, and 800 °C, respectively. The asymmetric CMS hollow fiber membranes had an outer diameter of ~265 μm and a separation layer ~5 μm on top of a porous substrate (Fig. 2a). The H_2/C_3H_8 separation performance (Fig. 2b–d) of CMS hollow fiber membranes was measured at 600 °C (furnace set temperature) using a 50%/50% H_2/C_3H_8 feed mixture at 1 bar.

As the pyrolysis temperature increased from 550 to 800 °C, the H_2/C_3H_8 separation factor increased by more than two orders of magnitude from 130 to 35177 with ~68% drop in H_2 permeance (Fig. 2e). Previous studies show that CMS ultramicropores are refined as the pyrolysis temperature increases [27], which is presumably responsible for the dramatically increased H_2/C_3H_8 separation factor. The refined ultramicropores can increase diffusion selectivity via enhancing molecule size discrimination (C_3H_8 kinetic diameter~4.3 Å vs H_2 kinetic diameter~2.9 Å). In addition, finer ultramicropores can increase sorption selectivity by excluding bulkier C_3H_8 molecules [57]. While diffusion selectivity normally reduces with increasing permeation temperature [58], such exclusion-mediated sorption selectivity is presumed to be independent of permeation temperature, and is possibly responsible for the ultra-high separation factors at 600 °C. Propane is much more condensable than hydrogen (critical temperature: 369.5 K vs 32.9 K), and competition effects are expected to compromise H_2/C_3H_8 separation factors under mixture permeation. The competition effects were likely suppressed due to reduced sorption under high-temperature permeation at 600 °C, which enabled the attractive H_2/C_3H_8 separation factors shown in Fig. 2. Notably, the CMS hollow fiber membranes pyrolyzed at 550 and 675 °C had almost identical H_2 permeances. This is possibly because CMS membrane prepared at 550 °C underwent further pyrolysis and pore structure change during permeation at 600 °C. Overall, the CMS hollow fiber membrane pyrolyzed at 675 °C provides a good balance between H_2 permeance and H_2/C_3H_8 separation factor, and was therefore chosen for more detailed studies on the effects of permeation temperature and feed composition.

4.2. Effects of permeation temperature on high-temperature H_2/C_3H_8 separation performance

Temperatures of catalytic membrane reactors are often chosen to maximize catalyst selectivity and product yield. It is important to understand the effects of permeation temperature on membrane high-temperature separation performance. The CMS hollow fiber membrane

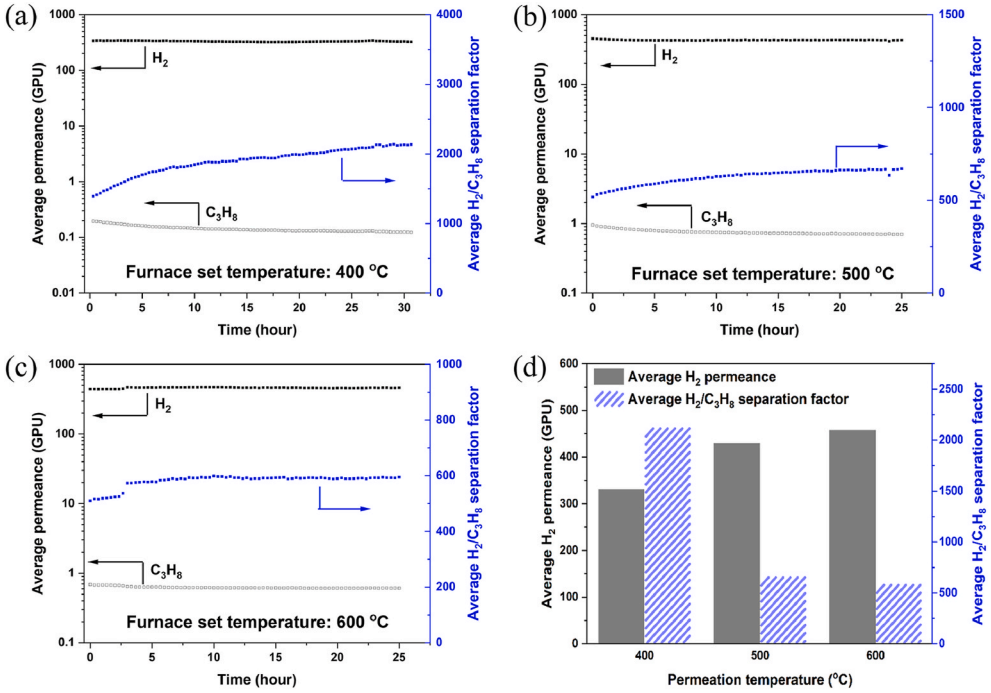

Fig. 3. H_2/C_3H_8 permeation results in CMS hollow fiber membranes measured at different furnace set temperatures (a) 400 °C, (b) 500 °C, and (c) 600 °C; (d) Stabilized average permeances and separation factors. The measurements were carried out using the CMS hollow fiber membrane pyrolyzed at 675 °C with a 50%H_2/50%C_3H_8 feed mixture (1 bar).

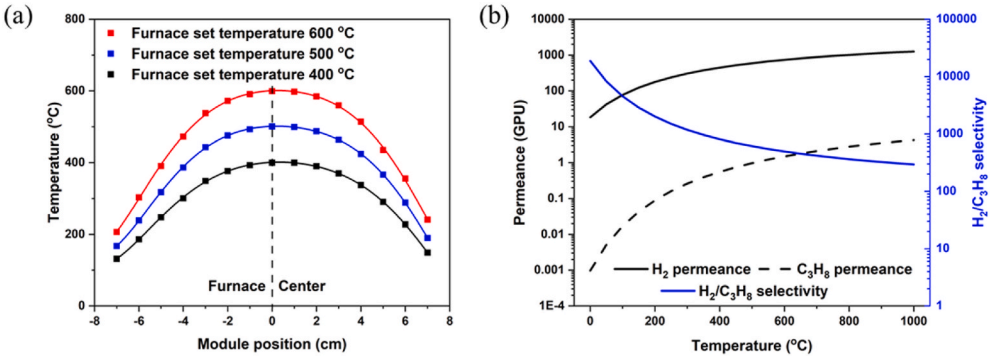

Fig. 4. (a) Furnace temperature distribution profiles (furnace length = 14 cm); (b) Calculated H_2 and C_3H_8 permeances and H_2/C_3H_8 selectivity at 0–1000 °C.

pyrolyzed at 675 °C was studied for H_2/C_3H_8 mixture (50%/50%) permeation at furnace set temperatures of 400, 500, and 600 °C (Fig. 3). As the temperature increased from 400 to 600 °C, the average H_2 permeance increased from 331 to 458 GPU while the average H_2/C_3H_8 separation factor decreased from 2127 to 591. It should be noted that the permeation test at 400 °C (Fig. 3a) required longer time (~27 h) to reach steady state possibly due to lower diffusivity at lower permeation temperature.

Since heating provided by the single-zone furnace (Fig. 1) was not uniform, average permeances and separation factors were obtained from the permeation measurements. To predict permeances and separation factors at a given temperature, temperature distribution profiles (Fig. 4a) inside the furnace were obtained at each furnace set temperature. The temperature at the furnace center was equal to the furnace set temperature and reduced towards the edge of the furnace. The measured average permeances and temperature distribution profiles allowed us to calculate (Eqn. (11)) H_2 and C_3H_8 apparent permeation activation energies using the least-squares method, which is 12.2 kJ/mol and 24.2 kJ/mol, respectively. The positive apparent permeation activation energies suggest high-temperature permeation of H_2 and C_3H_8 in the CMS membrane is dominated by diffusion. The apparent activation permeation energy of C_3H_8 is higher than that of C_2H_6 (19.0 kJ/mol), which was obtained from ambient temperature (25–50 °C) C_2H_6 permeation data measured in Matrimid®-derived CMS dense films pyrolyzed at 675 °C [58]. Using the obtained apparent permeation activation energies and pre-exponential factors, H_2 and C_3H_8 permeances and H_2/C_3H_8 selectivity at 0–1000 °C (Fig. 4b) were calculated using the Arrhenius equation (Eqn. (9)).

4.3. *Effects of feed composition on high-temperature H_2/C_3H_8 separation performance*

We studied the effects of feed composition on H_2/C_3H_8 separation performance of asymmetric CMS hollow fiber membranes at furnace set temperature of 600 °C (Fig. 5). The CMS hollow fiber membranes pyrolyzed at 675 °C were used for the permeation measurements. Five H_2/C_3H_8 feed mixtures were used: (A) 15%/85% H_2/C_3H_8; (B) 25%/75% H_2/C_3H_8; (C) 50%/50% H_2/C_3H_8; (D) 60%/40% H_2/C_3H_8; (E) 75%/25% H_2/C_3H_8. With feed A (15%/85% H_2/C_3H_8), the CMS hollow fiber membrane showed reduced average H_2 and C_3H_8 permeances and

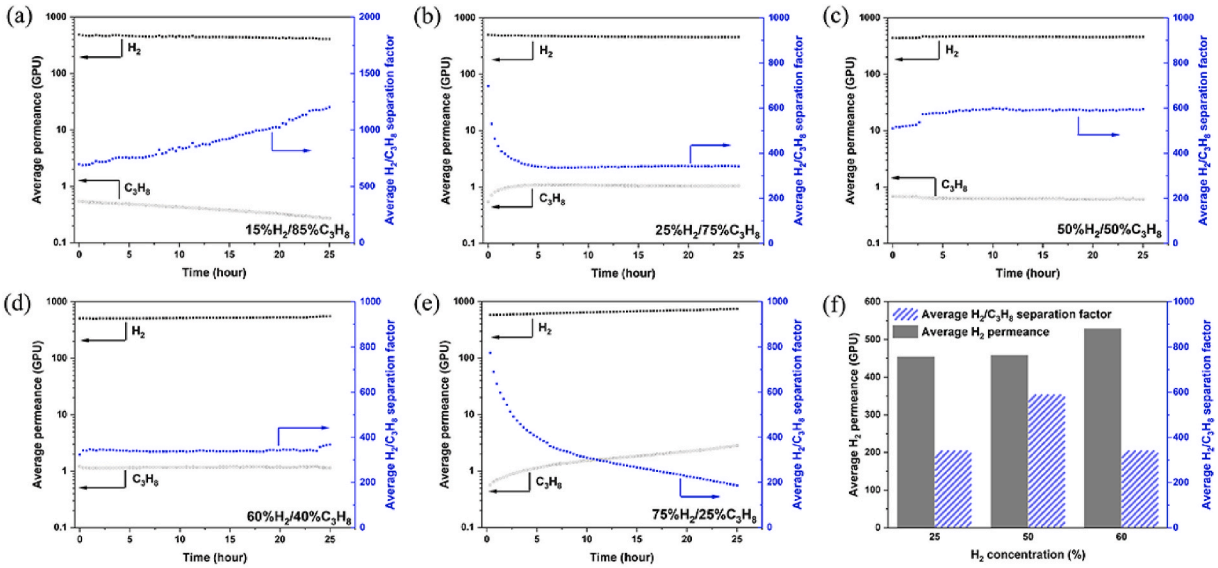

Fig. 5. H_2/C_3H_8 permeation results in CMS hollow fiber membranes using feed mixture (1 bar) comprising (a) 15%/85% H_2/C_3H_8, (b) 25%/75% H_2/C_3H_8, (c) 50%/50% H_2/C_3H_8, (d) 60%/40% H_2/C_3H_8, and (e) 75%/25% H_2/C_3H_8; (f) Stabilized average permeances and separation factors under feed (b), (c), and (d). The measurements were performed at 600 °C using the CMS hollow fiber membrane pyrolyzed at 675 °C.

Table 1
DFT pore surface area and pore volume (pore width <10.66 Å) of CMS films.

	Fresh CMS	C_3H_6-exposed CMS	H_2-exposed CMS
Pore surface area (m^2/g)	346.0	123.2	429.5
Pore volume (cm^3/g)	0.102	0.034	0.133

increased average H_2/C_3H_8 separation factor over time and a stable H_2/C_3H_8 separation factor cannot be obtained following 25 h (Fig. 5a). To understand the time-dependent permeation properties, we prepared CMS dense films using Matrimid® precursor dense films and exposed the CMS dense films to pure propylene (C_3H_6) at 600 °C. Following the C_3H_6 exposure, both the density functional theory (DFT) pore surface area and pore volume of the CMS dense film dramatically dropped (Table 1). We hypothesize gas-phase propane dehydrogenation reaction occurred in the CMS hollow fiber module feed side and produced C_3H_6, which is known as a coke precursor. Polymerization of adsorbed C_3H_6 molecules possibly caused deposition of carbonaceous materials (coke) in the CMS membrane pore network (Fig. 6a), thereby altering the membrane pore structure and permeation properties over time. Indeed, chemical vapor deposition of C_3H_6 and other hydrocarbons was used as a post-treatment tool to refine the pore size of CMS membranes and adsorbents [59,60].

With feed E (75%/25% H_2/C_3H_8), the CMS hollow fiber membrane showed increased H_2 and C_3H_8 permeances and reduced H_2/C_3H_8 separation factor over time (Fig. 5e). Hydrogen is known as a gasifying agent, which can remove carbonaceous deposits from coked catalysts via hydrogenation [61]. A recent report showed that mixing H_2 in pyrolysis purge gas can increase CMS pore sizes [34]. We hypothesize that adsorbed H_2 molecules can cause hydrogenation and thinning of the graphene sheets that constitute the CMS ultramicropores under high-temperature permeation (Fig. 6b), which increases CMS ultramicropore size. The enlarged CMS ultramicropores increase diffusivities and permeances while reducing the membrane diffusion selectivity and separation factor. To test this hypothesis, Matrimid®-derived CMS dense films were exposed to pure H_2 at 600 °C. Following H_2 exposure, the CMS dense film showed increased DFT pore surface area and pore volume (Table 1). Comparing the pore size distribution between fresh CMS dense film and H_2-exposed CMS dense film indicates that high-temperature H_2 exposure enlarged the CMS ultramicropores. Remarkably, the "fine" ultramicropores smaller than 5 Å disappeared following the high-temperature H_2 exposure (Fig. 6c). These results indicate that high-temperature H_2 exposure can be used as post-synthetic modification to tune the pore structure and separation performance of CMS membranes.

The CMS membrane structural changes by C_3H_6-induced coke deposition and H_2-dehydrogenation are not known to take place under room-temperature permeation. They are possibly unique to high-temperature permeation, in which both the membrane and the penetrants are more reactive. Notably, the asymmetric CMS hollow fiber membrane can provide stable high-temperature H_2/C_3H_8 separation performance under a comfortably wide feed composition window of

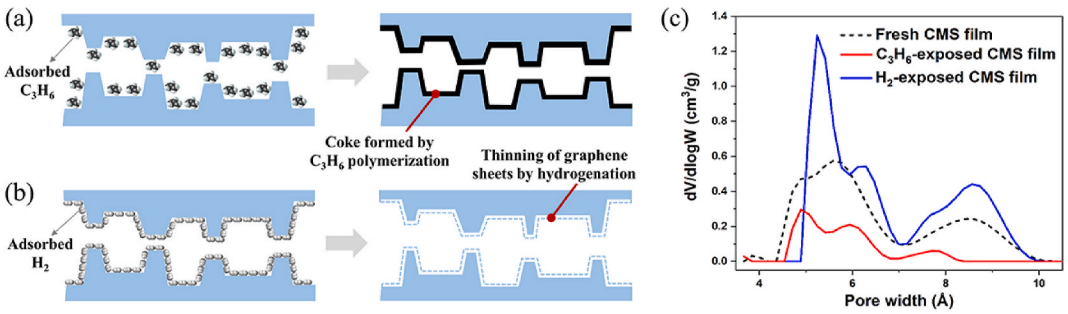

Fig. 6. Schematics showing hypothetical CMS pore structure changes as a result of (a) C_3H_6-induced coke deposition and (b) H_2-induced hydrogenation; (c) DFT pore size distribution of fresh CMS dense films and CMS dense films exposed to pure C_3H_6 and pure H_2.

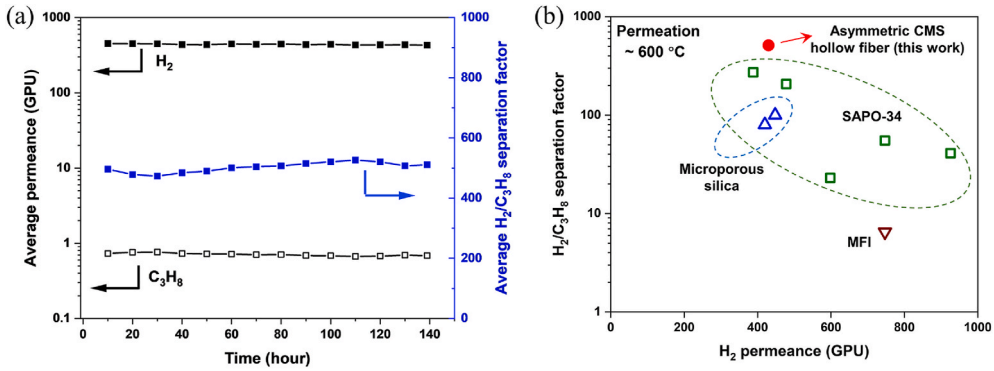

Fig. 7. (a) CMS hollow fiber membrane stability under a long-term (130 h) high-temperature (600 °C) permeation test. The test was carried out using a CMS hollow fiber membrane pyrolyzed at 675 °C under a 50%H_2/50%C_3H_8 feed mixture (1 bar); (b) Comparing high-temperature (600 °C) H_2/C_3H_8 separation performance of the CMS hollow fiber membrane studied in this work and microporous oxide membranes reported in literature [14,17,63–65].

25–60% H_2 (i.e., feed B, C, and D, Fig. 5b–d). The stable separation performance was presumably obtained by a dynamic equilibrium between competing C_3H_6-induced coke deposition and H_2-induced hydrogenation. The results suggest that asymmetric CMS hollow fiber membranes are potentially suitable for PDH membrane reactors under controlled reaction conditions. We speculate that the stable feed composition window is determined by permeation temperature, feed pressure, and CMS membrane pore structure, possibly among other factors. An in-depth study on these factors will undoubtedly be useful to further assess CMS membranes for PDH membrane reactor applications, however, is beyond the scope of this work.

4.4. *Membrane stability under long-term high-temperature permeation*

A CMS hollow fiber membrane module was constructed to study the membrane long-term stability under high-temperature H_2/C_3H_8 permeation. The permeation test was performed at 600 °C using the asymmetric CMS hollow fiber membrane pyrolyzed at 675 °C under 50%/50% H_2/C_3H_8 feed. Once steady state permeation was reached (~10 h), the membrane showed outstanding stability (Fig. 7a) under continuous permeation for ~130 h with average H_2 permeance of 430 GPU and average H_2/C_3H_8 separation factor of 511. Only a slight drop in average H_2 permeance (~4.7%) and an increase in average H_2/C_3H_8 separation factor (~3%) were observed during the course of the permeation test, which may be attributed to physical aging of the CMS membrane. Indeed, Qiu and co-workers showed that physical aging can occur even as CMS membranes are exposed to high temperatures [62]. Compared with microporous oxide membranes (e.g., zeolite [14,63,64], microporous silica [17,65]), the CMS hollow fiber membranes can provide ~2–100 folds higher H_2/C_3H_8 separation factors (Fig. 7b) and competitive H_2 permeances under similar permeation conditions at 600 °C.

5. Conclusions

For the first time, high-temperature permeation (up to 600 °C) in asymmetric CMS hollow fiber membranes with thin (~5 μm) separation layers was systematically investigated. The results suggest CMS hollow fiber membranes can provide attractive high-temperature H_2/C_3H_8 separation performance and hence are promising for propane dehydrogenation membrane reactor applications under controlled conditions. Under a continuous permeation test (~130 h) using a 50%/50% H_2/C_3H_8 feed mixture at 600 °C, the CMS hollow fiber membranes pyrolyzed at 675 °C showed average H_2 permeance of 430 GPU and H_2/C_3H_8 separation factor of 511 exceeding those of microporous oxide membranes. As the CMS hollow fiber membrane pyrolysis temperature increased, the average H_2 permeance decreased with increasing average H_2/C_3H_8 separation factors. We also found that CMS hollow fiber membrane permeances increase with increasing permeation temperature, suggesting high-temperature H_2/C_3H_8 permeation in CMS membranes is diffusion-controlled. The Arrhenius equation was used to calculate H_2 and C_3H_8 apparent permeation activation energies, which allowed us to estimate membrane intrinsic H_2/C_3H_8 permeation properties at given temperatures. Finally, feed composition was found to affect the stability of high-temperature H_2/C_3H_8 permeation in CMS hollow fiber membranes, which was not seen for room-temperature permeation. A stable feed composition window of 25–60% H_2 was identified under the studied conditions, outside of which time-dependent permeation was observed presumably due to CMS membrane pore structure change as a result of hydrogenation or coking.

Declaration of competing interest

The authors declare the following financial interests/personal relationships which may be considered as potential competing interests: Chen Zhang reports financial support was provided by National Science Foundation.

Acknowledgements

This work is supported by funding from National Science Foundation (CBET Award No.1928325). L.L. acknowledges the Hulka Energy Research Fellowship provided through the Maryland Energy Innovation Institute. C.Z. thanks additional faculty summer support from the Minta Martin Foundation. The authors thank the Huntsman Corporation for kindly providing Matrimid® polymer samples.

Appendix A. Supplementary data

Supplementary data to this article can be found online at https://doi.org/10.1016/j.memsci.2021.119978.

Credit author statement

Lu Liu: Methodology, Investigation, Validation, Formal analysis, Writing - Original Draft, Writing - Review & Editing. **Dongxia Liu:** Conceptualization, Funding acquisition, Supervision, Project administration, Writing - Review & Editing. **Chen Zhang:** Conceptualization, Funding acquisition, Supervision, Project administration, Writing - Review & Editing.

References

[1] G. Saracco, H. Neomagus, G. Versteeg, W.P.M. van Swaaij, High-temperature membrane reactors: potential and problems, Chem. Eng. Sci. 54 (1999) 1997–2017.

[2] N. Itoh, W.-C. Xu, K. Haraya, Basic experimental study on palladium membrane reactors, J. Membr. Sci. 66 (1992) 149–155.
[3] P. Ciavarella, D. Casanave, H. Moueddeb, S. Miachon, K. Fiaty, J.-A. Dalmon, Isobutane dehydrogenation in a membrane reactor: influence of the operating conditions on the performance, Catal. Today 67 (2001) 177–184.
[4] A. Basile, E. Drioli, F. Santell, V. Violante, G. Capannelli, G. Vitulli, A study on catalytic membrane reactors for water gas shift reaction, Gas Sep. Purif. 10 (1996) 53–61.
[5] A. Arvanitis, X. Sun, S. Yang, D. Damma, P. Smirniotis, J. Dong, Approaching complete CO conversion and total H_2 recovery for water gas shift reaction in a high-temperature and high-pressure zeolite membrane reactor, J. Membr. Sci. 549 (2018) 575–580.
[6] A. Iulianelli, P. Ribeirinha, A. Mendes, A. Basile, Methanol steam reforming for hydrogen generation via conventional and membrane reactors: a review, Renew. Sustain. Energy Rev. 29 (2014) 355–368.
[7] F. Gallucci, L. Paturzo, A. Basile, An experimental study of CO_2 hydrogenation into methanol involving a zeolite membrane reactor, Chem. Eng. Process. Process Intensif. 43 (2004) 1029–1036.
[8] S. Pati, J. Ashok, N. Dewangan, T. Chen, S. Kawi, Ultra-thin (~ 1 μm) Pd–Cu membrane reactor for coupling CO_2 hydrogenation and propane dehydrogenation applications, J. Membr. Sci. 595 (2020) 117496.
[9] R.h. Yuan, Z. He, Y. Zhang, W.d. Wang, C.s. Chen, H. Wu, Z.l. Zhan, Partial oxidation of methane to syngas in a packed bed catalyst membrane reactor, AIChE J. 62 (2016) 2170–2176.
[10] A. Basile, L. Paturzo, F. Laganà, The partial oxidation of methane to syngas in a palladium membrane reactor: simulation and experimental studies, Catal. Today 67 (2001) 65–75.
[11] M. Sakbodin, Y. Wu, S.C. Oh, E.D. Wachsman, D. Liu, Hydrogen-permeable tubular membrane reactor: promoting conversion and product selectivity for non-oxidative activation of methane over an Fe©SiO2 catalyst, Angew. Chem. Int. Ed. 55 (2016) 16149–16152.
[12] Z. Nawaz, Light alkane dehydrogenation to light olefin technologies: a comprehensive review, Rev. Chem. Eng. 31 (2015) 413–436.
[13] J.J. Sattler, J. Ruiz-Martinez, E. Santillan-Jimenez, B.M. Weckhuysen, Catalytic dehydrogenation of light alkanes on metals and metal oxides, Chem. Rev. 114 (2014) 10613–10653.
[14] S.-J. Kim, Y. Liu, J.S. Moore, R.S. Dixit, J.G. Pendergast Jr., D. Sholl, C.W. Jones, S. Nair, Thin hydrogen-selective SAPO-34 zeolite membranes for enhanced conversion and selectivity in propane dehydrogenation membrane reactors, Chem. Mater. 28 (2016) 4397–4402.
[15] H. Weyten, K. Keizer, A. Kinoo, J. Luyten, R. Leysen, Dehydrogenation of propane using a packed-bed catalytic membrane reactor, AIChE J. 43 (1997) 1819–1827.
[16] R. Schäfer, M. Noack, P. Kölsch, S. Thomas, A. Seidel-Morgenstern, J. Caro, Development of a H_2-selective SiO_2-membrane for the catalytic dehydrogenation of propane, Separ. Purif. Technol. 25 (2001) 3–9.
[17] H. Weyten, J. Luyten, K. Keizer, L. Willems, R. Leysen, Membrane performance: the key issues for dehydrogenation reactions in a catalytic membrane reactor, Catal. Today 56 (2000) 3–11.
[18] P. Quicker, V. Höllein, R. Dittmeyer, Catalytic dehydrogenation of hydrocarbons in palladium composite membrane reactors, Catal. Today 56 (2000) 21–34.
[19] Z. Wang, Z. Bian, N. Dewangan, J. Xu, S. Kawi, High-performance catalytic perovskite hollow fiber membrane reactor for oxidative propane dehydrogenation, J. Membr. Sci. 578 (2019) 36–42.
[20] O. Czuprat, S. Werth, J. Caro, T. Schiestel, Oxidative dehydrogenation of propane in a perovskite membrane reactor with multi-step oxygen insertion, AIChE J. 56 (2010) 2390–2396.
[21] J. Xu, K.-G. Haw, Z. Li, S. Pati, Z. Wang, S. Kawi, A mini-review on recent developments in SAPO-34 zeolite membranes and membrane reactors, React. Chem. Eng. 6 (2021) 52–66.
[22] M. Rungta, C. Zhang, W.J. Koros, L. Xu, Membrane-based ethylene/ethane separation: the upper bound and beyond, AIChE J. 59 (2013) 3475–3489.
[23] L. Xu, M. Rungta, W.J. Koros, Matrimid® derived carbon molecular sieve hollow fiber membranes for ethylene/ethane separation, J. Membr. Sci. 380 (2011) 138–147.
[24] S.L. Touma, J.C. Vaz, F.C. De Almeida Rego, V.A. Barros, J.F. Do Nascimento, M.d. C. Amaral, E.C. De Miranda Costa, A.F.F. De Souza, Innovative gas treatment solutions for offshore systems, in: Offshore Technology Conference Brasil, 2019.
[25] L. Lei, A. Lindbråthen, M. Hillestad, X. He, Carbon molecular sieve membranes for hydrogen purification from a steam methane reforming process, J. Membr. Sci. 627 (2021) 119241.
[26] M. Rungta, G.B. Wenz, C. Zhang, L. Xu, W. Qiu, J.S. Adams, W.J. Koros, Carbon molecular sieve structure development and membrane performance relationships, Carbon 115 (2017) 237–248.
[27] X. Ning, W.J. Koros, Carbon molecular sieve membranes derived from Matrimid® polyimide for nitrogen/methane separation, Carbon 66 (2014) 511–522.
[28] P.T. Ngamou, M. Ivanova, O. Guillon, W.A. Meulenberg, High-performance carbon molecular sieve membranes for hydrogen purification and pervaporation dehydration of organic solvents, J. Mater. Chem. 7 (2019) 7082–7091.
[29] M. Hou, W. Qi, L. Li, R. Xu, J. Xue, Y. Zhang, C. Song, T. Wang, Carbon molecular sieve membrane with tunable microstructure for CO_2 separation: effect of multiscale structures of polyimide precursors, J. Membr. Sci. (2021) 119541.
[30] H.J. Yu, J.H. Shin, A.S. Lee, S.S. Hwang, J.-H. Kim, S. Back, J.S. Lee, Tailoring selective pores of carbon molecular sieve membranes towards enhanced N_2/CH_4 separation efficiency, J. Membr. Sci. 620 (2021) 118814.
[31] S.-J. Kim, J.F. Kim, Y.H. Cho, S.-E. Nam, H. Park, Y.-I. Park, Aging-resistant carbon molecular sieve membrane derived from pre-crosslinked Matrimid® for propylene/propane separation, J. Membr. Sci. 636 (2021) 119555.
[32] S.L. Fu, E.S. Sanders, S.S. Kulkarni, W.J. Koros, Carbon molecular sieve membrane structure-property relationships for four novel 6FDA based polyimide precursors, J. Membr. Sci. 487 (2015) 60–73.
[33] C. Zhang, G.B. Wenz, P.J. Williams, J.M. Mayne, G. Liu, W.J. Koros, Purification of aggressive supercritical natural gas using carbon molecular sieve hollow fiber membranes, Ind. Eng. Chem. Res. 56 (2017) 10482–10490.
[34] Y. Ma, M.L. Jue, F. Zhang, R. Mathias, H.Y. Jang, R.P. Lively, Creation of well-defined "mid-sized" micropores in carbon molecular sieve membranes, Angew. Chem. Int. Ed. 131 (2019) 13393–13399.
[35] X. Ma, Y.S. Lin, X. Wei, J. Kniep, Ultrathin carbon molecular sieve membrane for propylene/propane separation, AIChE J. 62 (2016) 491–499.
[36] D.-Y. Koh, B.A. McCool, H.W. Deckman, R.P. Lively, Reverse osmosis molecular differentiation of organic liquids using carbon molecular sieve membranes, Science 353 (2016) 804–807.
[37] G.A. Sznejer, I. Efremenko, M. Sheintuch, Carbon membranes for high temperature gas separations: experiment and theory, AIChE J. 50 (2004) 596–610.
[38] N. Itoh, K. Haraya, A carbon membrane reactor, Catal. Today 56 (2000) 103–111.
[39] G. Sznejer, M. Sheintuch, Application of a carbon membrane reactor for dehydrogenation reactions, Chem. Eng. Sci. 59 (2004) 2013–2021.
[40] Y. Hirota, A. Ishikado, Y. Uchida, Y. Egashira, N. Nishiyama, Pore size control of microporous carbon membranes by post-synthesis activation and their use in a membrane reactor for dehydrogenation of methylcyclohexane, J. Membr. Sci. 440 (2013) 134–139.
[41] M. Abdollahi, J. Yu, P.K. Liu, R. Ciora, M. Sahimi, T.T. Tsotsis, Hydrogen production from coal-derived syngas using a catalytic membrane reactor based process, J. Membr. Sci. 363 (2010) 160–169.
[42] A. Harale, H.T. Hwang, P.K. Liu, M. Sahimi, T.T. Tsotsis, Experimental studies of a hybrid adsorbent-membrane reactor (HAMR) system for hydrogen production, Chem. Eng. Sci. 62 (2007) 4126–4137.
[43] S. Sá, J.M. Sousa, A. Mendes, Steam reforming of methanol over a $CuO/ZnO/Al_2O_3$ catalyst part II: a carbon membrane reactor, Chem. Eng. Sci. 66 (2011) 5523–5530.
[44] X. Zhang, H. Hu, Y. Zhu, S. Zhu, Methanol steam reforming to hydrogen in a carbon membrane reactor system, Ind. Eng. Chem. Res. 45 (2006) 7997–8001.
[45] N. Bhuwania, Y. Labreche, C.S. Achoundong, J. Baltazar, S.K. Burgess, S. Karwa, L. Xu, C.L. Henderson, P.J. Williams, W.J. Koros, Engineering substructure morphology of asymmetric carbon molecular sieve hollow fiber membranes, Carbon 76 (2014) 417–434.
[46] C. Zhang, K. Zhang, Y. Cao, W.J. Koros, Composite carbon molecular sieve hollow fiber membranes: resisting support densification via silica particle stabilization, Ind. Eng. Chem. Res. 57 (2018) 16051–16058.
[47] C. Zhang, R. Kumar, W.J. Koros, Ultra-thin skin carbon hollow fiber membranes for sustainable molecular separations, AIChE J. 65 (2019), e16611.
[48] W.J. Koros, R.P. Lively, Water and beyond: expanding the spectrum of large-scale energy efficient separation processes, AIChE J. 58 (2012) 2624–2633.
[49] W.J. Koros, C. Zhang, Materials for next-generation molecularly selective synthetic membranes, Nat. Mater. 16 (2017) 289–297.
[50] W.J. Koros, G. Fleming, Membrane-based gas separation, J. Membr. Sci. 83 (1993) 1–80.
[51] Y. Ma, F. Zhang, S. Yang, R.P. Lively, Evidence for entropic diffusion selection of xylene isomers in carbon molecular sieve membranes, J. Membr. Sci. 564 (2018) 404–414.
[52] L. Xu, C. Zhang, M. Rungta, W. Qiu, J. Liu, W.J. Koros, Formation of defect-free 6FDA-DAM asymmetric hollow fiber membranes for gas separations, J. Membr. Sci. 459 (2014) 223–232.
[53] L. Xu, in: Ph.D. Dissertation, Georgia Institute of Technology, 2012.
[54] D.T. Clausi, W.J. Koros, Formation of defect-free polyimide hollow fiber membranes for gas separations, J. Membr. Sci. 167 (2000) 79–89.
[55] C. Zhang, Y. Dai, J.R. Johnson, O. Karvan, W.J. Koros, High performance ZIF-8/6FDA-DAM mixed matrix membrane for propylene/propane separations, J. Membr. Sci. 389 (2012) 34–42.
[56] D.Q. Vu, W.J. Koros, S.J. Miller, High pressure CO_2/CH_4 separation using carbon molecular sieve hollow fiber membranes, Ind. Eng. Chem. Res. 41 (2002) 367–380.
[57] C. Zhang, W.J. Koros, Ultraselective carbon molecular sieve membranes with tailored synergistic sorption selective properties, Adv. Mater. 29 (2017) 1701631.
[58] M. Rungta, in: Ph.D. Dissertation, Georgia Institute of Technology, 2012.
[59] M. Yoshimune, K. Haraya, Simple control of the pore structures and gas separation performances of carbon hollow fiber membranes by chemical vapor deposition of propylene, Separ. Purif. Technol. 223 (2019) 162–167.
[60] S. Haider, A. Lindbråthen, J.A. Lie, I.C.T. Andersen, M.-B. Hägg, CO_2 separation with carbon membranes in high pressure and elevated temperature applications, Separ. Purif. Technol. 190 (2018) 177–189.
[61] J. Zhou, J. Zhao, J. Zhang, T. Zhang, M. Ye, Z. Liu, Regeneration of catalysts deactivated by coke deposition: a review, Chin. J. Catal. 41 (2020) 1048–1061.
[62] W. Qiu, J. Vaughn, G. Liu, L. Xu, M. Brayden, M. Martinez, T. Fitzgibbons, G. Wenz, W.J. Koros, Hyperaging tuning of a carbon molecular sieve hollow fiber membrane with extraordinary gas separation performance and stability, Angew. Chem. Int. Ed. 58 (2019) 11700–11703.
[63] S.-J. Kim, S. Tan, M. Taborga Claure, L. Briones Gil, K.L. More, Y. Liu, J.S. Moore, R.S. Dixit, J.G. Pendergast, D.S. Sholl, C.W. Jones, S. Nair, One-step synthesis of

zeolite membranes containing catalytic metal nanoclusters, ACS Appl. Mater. Interfaces 8 (2016) 24671–24681.

[64] Z. Wang, J. Xu, S. Pati, T. Chen, Y. Deng, N. Dewangan, L. Meng, J.Y.S. Lin, S. Kawi, High H_2 permeable SAPO-34 hollow fiber membrane for high temperature propane dehydrogenation application, AIChE J. 66 (2020), e16278.

[65] K. Ishii, A. Shibata, T. Takeuchi, J. Yoshiura, T. Urabe, Y. Kameda, M. Nomura, Development of silica membranes to improve dehydration reactions, J. Jpn. Petrol. Inst. 62 (2019) 211–219.